

Measurement of differential cross sections of neutron-induced deuteron production reactions on carbon from 25 to 52 MeV*

Zengqi Cui(崔增琪)¹ Haoyu Jiang(江浩雨)¹ Kang Sun(孙康)^{2,3,4} Guohui Zhang(张国辉)^{1†} Ruirui Fan(樊瑞睿)^{2,3,5‡}
 Wei Jiang(蒋伟)^{2,3} Huaiyong Bai(白怀勇)¹ Yiwei Hu(胡益伟)¹ Jie Liu(刘杰)¹ Han Yi(易晗)^{2,3}
 Changjun Ning(宁常军)^{2,3} Zhijia Sun(孙志嘉)^{2,3,5} Jingyu Tang(唐靖宇)^{2,3} Qi An(安琪)^{5,6} Jie Bao(鲍杰)⁷
 Yu Bao(鲍煜)^{2,3} Ping Cao(曹平)^{5,6} Haolei Chen(陈昊磊)^{5,6} Qiping Chen(陈琪萍)⁸ Yonghao Chen(陈永浩)^{2,3}
 Yukai Chen(陈裕凯)^{2,3} Zhen Chen(陈朕)^{5,6} Changqing Feng(封常青)^{5,6} Keqing Gao(高可庆)^{2,3}
 Minhao Gu(顾旻皓)^{2,5} Changcai Han(韩长材)⁹ Zijie Han(韩子杰)⁸ Guozhu He(贺国珠)⁷
 Yongcheng He(何泳成)^{2,3} Yang Hong(洪杨)^{2,3,4} Hanxiong Huang(黄翰雄)⁷ Weiling Huang(黄蔚玲)^{2,3}
 Xiru Huang(黄锡汝)^{5,6} Xiaolu Ji(季筱路)^{2,5} Xuyang Ji(吉旭阳)^{5,10} Zhijie Jiang(姜智杰)^{5,6} Hantao Jing(敬罕涛)^{2,3}
 Ling Kang(康玲)^{2,3} Mingtao Kang(康明涛)^{2,3} Bo Li(李波)^{2,3} Chao Li(李超)^{5,6} Jiawen Li(李嘉雯)^{5,10}
 Lun Li(李论)^{2,3} Qiang Li(李强)^{2,3} Xiao Li(李晓)^{2,3} Yang Li(李祥)^{2,3} Rong Liu(刘荣)⁸ Shubin Liu(刘树彬)^{5,6}
 Xingyan Liu(刘星言)⁸ Guangyuan Luan(栾广源)⁷ Qili Mu(穆奇丽)^{2,3} Binbin Qi(齐斌斌)^{5,6} Jie Ren(任杰)⁷
 Zhizhou Ren(任智洲)^{6,8} Xichao Ruan(阮锡超)⁷ Zhaohui Song(宋朝晖)⁹ Yingpeng Song(宋英鹏)^{2,3}
 Hong Sun(孙虹)^{2,3} Xiaoyang Sun(孙晓阳)^{2,3,4} Zhixin Tan(谭志新)^{2,3} Hongqing Tang(唐洪庆)⁷
 Xinyi Tang(唐新懿)^{5,6} Binbin Tian(田斌斌)^{2,3} Lijiao Wang(王丽娇)^{2,3,4} Pengcheng Wang(王鹏程)^{2,3}
 Qi Wang(王琦)⁷ Taofeng Wang(王涛峰)¹¹ Zhaohui Wang(王朝辉)⁷ Jie Wen(文杰)⁸ Zhongwei Wen(温中伟)⁸
 Qingbiao Wu(吴青彪)^{2,3} Xiaoguang Wu(吴晓光)⁷ Xuan Wu(吴煊)^{2,3} Likun Xie(解立坤)^{5,10} Yiwei Yang(羊奕伟)⁸
 Li Yu(于莉)^{2,3} Tao Yu(余滔)^{5,6} Yongji Yu(于永积)^{2,3} Linhao Zhang(张林浩)^{2,3,4} Qiwei Zhang(张奇玮)⁷
 Xianpeng Zhang(张显鹏)⁹ Yuliang Zhang(张玉亮)^{2,3} Zhiyong Zhang(张志永)^{5,6} Yubin Zhao(赵豫斌)^{2,3}
 Luping Zhou(周路平)^{2,3,4} Zuying Zhou(周祖英)⁷ Danyang Zhu(朱丹阳)^{5,6} Kejun Zhu(朱科军)^{2,4,5}
 Peng Zhu(朱鹏)^{2,3}

(The CSNS Back-n Collaboration)

¹State Key Laboratory of Nuclear Physics and Technology, School of Physics, Peking University, Beijing 100871, China

²Institute of High Energy Physics, Chinese Academy of Sciences (CAS), Beijing 100049, China

³Spallation Neutron Source Science Center, Dongguan 523803, China

⁴University of Chinese Academy of Sciences, Beijing 100049, China

⁵State Key Laboratory of Particle Detection and Electronics

⁶Department of Modern Physics, University of Science and Technology of China, Hefei 230026, China

⁷Key Laboratory of Nuclear Data, China Institute of Atomic Energy, Beijing 102413, China

⁸Institute of Nuclear Physics and Chemistry, China Academy of Engineering Physics, Mianyang 621900, China

⁹Northwest Institute of Nuclear Technology, Xi'an 710024, China

¹⁰Department of Engineering and Applied Physics, University of Science and Technology of China, Hefei 230026, China

¹¹School of Physics, Beihang University, Beijing 100083, China

Abstract: The angle-differential cross sections of neutron-induced deuteron production from carbon were measured at six neutron energies from 25 to 52 MeV relative to those of n - p elastic scattering at the China Spallation Neutron Source (CSNS) Back-n white neutron source. By employing the ΔE - E telescopes of the Light-charged Particle Detector Array (LPDA) system at 15.1° to 55.0° in the laboratory system, ratios of the angle-differential cross sections of the $^{12}\text{C}(n, xd)$ reactions to those of the n - p scattering were measured, and then, the angle-differential cross sections of the $^{12}\text{C}(n, xd)$ reactions were obtained using the angle-differential cross sections of the n - p elastic scattering from the JENDL-4.0/HE-2015 library as the standard. The obtained results are compared with data from previous measurements, all of which are based on mono-energetic neutrons, the evaluated data from the JENDL-4.0/

Received 29 January 2021; Accepted 23 March 2021; Published online 27 April 2021

* Supported by the National Natural Science Foundation of China (11775006) and the National Key R&D Program of China (2016YFA0401604)

† E-mail: guohuizhang@pku.edu.cn

‡ E-mail: fanrr@ihep.ac.cn

©2021 Chinese Physical Society and the Institute of High Energy Physics of the Chinese Academy of Sciences and the Institute of Modern Physics of the Chinese Academy of Sciences and IOP Publishing Ltd

HE-2015 library and the ENDF-B/VIII.0 library, and those from theoretical calculations based on INCA code and Talys-1.9 code. Being the first white-neutron-source-based systematic measurement of the angle-differential cross sections of neutron-induced deuteron production reactions on carbon in several tens of MeV, the present work can provide a reference to the data library considering the lack of experimental data.

Keywords: $^{12}\text{C}(n, xd)$ reactions, relative angle-differential cross sections, CSNS Back-n white neutron source, LPDA

DOI: 10.1088/1674-1137/abf136

I. INTRODUCTION

The neutron-induced light-charged particle emitting reactions of carbon in several tens of MeV neutron energy, i.e., $^{12}\text{C}(n, lcp)$ reactions, can offer information about the nuclear structure, and their angle-differential cross section (hereinafter referred to as differential cross section) data are needed to test the nuclear reaction models [1, 2]. Among these (n, lcp) reactions, deuteron production ($^{12}\text{C}(n, xd)$) reactions are rather crucial because their differential cross sections are required for dose calculations in human tissues for fast neutron cancer therapy and cosmic-ray-induced neutrons considering the large amount of carbon in human tissues [1, 3-8]. Meanwhile, charged particle production reactions are of great significance to nuclear detection. Taking carbon-based neutron detectors such as plastic scintillator detectors as an example [9], precise cross sections and differential cross sections of $^{12}\text{C}(n, xd)$ reactions are required in the simulation of the response of the detectors to fast neutrons. In addition, the cross sections of the $^{12}\text{C}(n, d_0)^{11}\text{B}$ and $^{12}\text{C}(n, d_1)^{11}\text{B}$ reactions were measured by Pillon *et al.* [10], and the cross section of the $^{12}\text{C}(n, d_0)^{11}\text{B}$ reaction was recently measured by Majerle *et al.* [11]. Diamond detectors were used in both measurements, which suggests that deuteron production reactions can contribute to the response of diamond detectors. This importance necessitates the study of the differential cross sections of $^{13}\text{C}(n, xd)$ reactions, which are referred to as $^{12}\text{C}(n, xd)$ reactions hereinafter in accordance with literature because of the dominance of ^{12}C over ^{13}C in abundance (98.93% vs 1.07%) [12].

However, the cross sections of the $^{12}\text{C}(n, xd)$ reactions are rather small, which creates difficulties in their measurement [13]. There are nine previous measurements [14], seven of which are in the several tens of MeV range: the works by Slypen *et al.* at $E_n = 29.5$ to 72.8 MeV [13, 15], as well as those by Subramanian *et al.* at $E_n = 27.4$ to 60.7 MeV [16], Tippawan *et al.* at $E_n = 95.6$ MeV [1], Bergenwall *et al.* at $E_n = 95.6$ MeV [2], McNaughton *et al.* at $E_n = 56.0$ MeV [9], and Nauchi *et al.* at $E_n = 64.5$ and 75.0 MeV [17] were all aimed at the measurement of the double differential cross sections of $^{12}\text{C}(n, xd)$ reactions, while the work by Young *et al.* for $E_n = 60.0$ MeV [18] was aimed in particular at the meas-

urement of the differential cross sections of the $^{12}\text{C}(n, d)^{11}\text{B}$ reaction. All seven measurements under 100 MeV were carried out on $^7\text{Li}(p, n)$ mono-energetic neutron sources. The results from previous measurements agree in trend but relatively large discrepancies in magnitude exist in some of them. For example, McNaughton's experimental data at $E_n = 56.0$ MeV [9] are considerably larger than Slypen's at $E_n = 55.3$ [13] MeV and at forward deuteron angles. Brenner *et al.* carried out comprehensive theoretical calculations of double differential cross sections by using intranuclear cascade (INCA) code [19], and there are some discrepancies between the theoretical calculations and experimental results [13]. Therefore, more measurements are needed, especially measurements using a white neutron source, which can provide systematicness. The China Spallation Neutron Source (CSNS) Back-n white neutron source provides neutrons of a wide energy range, which is suitable for measurements of neutron-induced nuclear reaction data [20].

In the present work, differential cross sections of $^{12}\text{C}(n, xd)$ reactions relative to those of n - p elastic scattering were measured at six neutron energies from 25 to 52 MeV. A graphite foil and a polyethylene foil were used as samples for the $^{12}\text{C}(n, xd)$ reactions and the n - p scattering measurements, respectively. The ΔE - E telescopes of the Light-charged Particle Detector Array (LPDA) system, each consisting of a Si-PIN detector (ΔE unit) and a CsI detector (E unit) placed in the forward direction from 10.1° to 55.0° with respect to the incident neutron, were employed. Measurements of the carbon sample for the $^{12}\text{C}(n, xd)$ reactions and the polyethylene sample for the n - p elastic scattering were performed. Ratios of the differential cross sections of the $^{12}\text{C}(n, xd)$ reactions to those of the n - p scattering were measured, and then the differential cross sections of the $^{12}\text{C}(n, xd)$ reactions were obtained using the differential cross sections of the n - p scattering [21] from the JENDL-4.0/HE-2015 library [22] as the standard.

II. EXPERIMENTAL SETUP

A. Neutron Source

The measurements were performed at Endstation #1 (ES#1) of the CSNS Back-n white neutron source [23].

Protons accelerated up to 1.6 GeV in the Rapid Cycling Synchrotron (RCS) impinged on a tungsten target with a repetition rate of 25 Hz and thus produce spallation neutrons. The Back-n beamline provided neutrons of a wide energy spectrum (from \sim eV to higher than 100 MeV) while the interference of the charged particles emitted from the tungsten target was eliminated by the bending magnet. The neutron source operated in double-bunch mode, with the time width of each proton bunch \sim 43 ns, and the separation duration between the two proton bunches was 410 ns [24]. The beam power during the present experiment was 50 kW. The neutron flight path was 57.99 m from the source to the sample. The diameter of the neutron beam spot was approximately 15 mm, and the neutron flux was $\sim 9.35 \times 10^5$ n/cm²/s. More details about the facility are presented in Ref. [25].

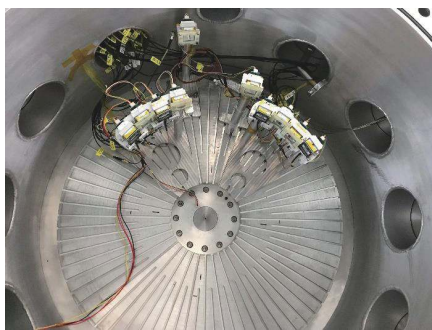
B. Samples

A picture of the samples and the sample holder is shown in Fig. 1.

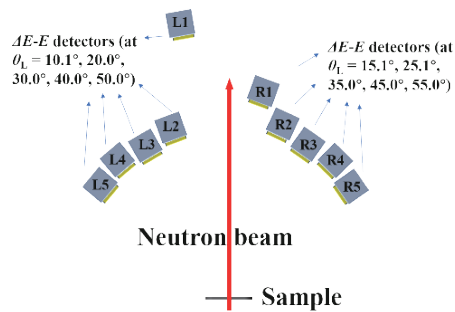
Four samples were used for the measurement: a high-purity graphite foil (carbon sample) of ~ 8.82 $\mu\text{g}/\text{cm}^2$ thickness for the foreground measurement of the $^{12}\text{C}(n, \alpha d)$ reactions, a low-density polyethylene (CH₂) sample of ~ 9.48 $\mu\text{g}/\text{cm}^2$ thickness for the n - p scattering measurement, an empty target for instrumental and neutron beam background measurement, and α sources for signal tests for the detectors, their electronics, and the data acquisition (DAQ) system. The α sources were back-to-back



Fig. 1. (color online) Samples and sample holder. From left to right: carbon sample, empty target, CH₂ sample, and α sources.



(a)



(b)

Fig. 2. (color online) (a) Picture of the interior of the LPDA vacuum chamber. (b) Schematic of the experimental setup.

²⁴¹Am sources, each with ~ 33 kBq activity. All the samples were mounted onto a customized aluminum holder, which has four sample positions. Three of them are rounded squares of 76.8 mm in side length for the graphite foil, empty target, and CH₂ sample, and one is a rectangle for the α sources. Therefore, the incident neutron beam spot was well covered by the sample (15 mm vs 76.8 mm).

C. Detectors

The measurement of the charged particles was achieved using the LPDA detector system. A picture of the interior of the LPDA vacuum chamber and the configuration of the detectors are presented in Fig. 2 (a) and (b), respectively. Ten sets of ΔE - E telescopes of the LPDA system were used in the vacuum chamber. Each telescope is composed of a 300 μm -thick Si-PIN detector (ΔE unit) and a 30 mm-thick CsI scintillator (E unit). The signals from each Si-PIN detector were amplified and pre-processed by a Mesytec MSI-8 amplifier [26], while the signals from each CsI detector were multiplied by a silicon photomultiplier (SiPM) [27] and then processed by a main amplifier. Detailed descriptions of the LPDA system and the electronics can be found in Refs. [28, 29]. The telescopes were placed in the forward direction from 10.1° to 55.0° with respect to the incident neutron beamline. The telescopes at the angles $\theta_L = 10.1^\circ, 20.0^\circ, \dots, 50.0^\circ$ (denoted as L1, L2, ..., L5) were placed on the left side of the neutron beamline while the other five sets of telescopes at $\theta_L = 15.1^\circ, 25.1^\circ, \dots, 55.0^\circ$ (denoted as R1, R2, ..., R5) were placed on the right. The distances between the centers of the detectors and the center of the sample are listed in Table 1. The detectors at $\theta_L = 10.1^\circ$ and $\theta_L = 15.1^\circ$ were located further away from the sample than the others to avoid the irradiation by the neutron beam. The solid angle and the average detection angle for each telescope were calculated from Monte Carlo simulation [30] and are listed in Table 1. Note that the surface of each sample was perpendicular to the direction of the incident neutron beam throughout the experiment.

Table 1. Geometric parameters of the LPDA ΔE - E telescopes.

Telescope	L1	L2	L3	L4	L5	R1	R2	R3	R4	R5
Detection Angle ($^\circ$) ^a	10.1	20.0	30.0	40.0	50.0	15.1	25.1	35.0	45.0	55.0
Distance (cm) ^b	41.0	24.9	24.0	24.9	24.0	29.0	24.0	24.9	24.0	24.9
Solid Angle (0.01 sr) ^c	0.3675	0.4997	1.0620	0.9900	1.0657	0.7331	1.0599	0.9891	1.0674	0.9868

a: Detection angle, the average angle for each telescope according to Monte Carlo simulation. b: Distance, the distance between the center of each Si detector and the center of the sample. c: Solid angle of each telescope, calculated from Monte Carlo simulation (in 0.01 sr).

D. Experimental procedure

The total beam duration for the measurement was approximately 210 h, split into seven rounds each consisting of ~ 18 h of CH_2 measurement, ~ 6 h of graphite measurement, and ~ 0.5 h of empty target measurement. Since the experiment was originally intended for the measurement of n - p scattering and the graphite measurement served as the background run [21], the measurement duration for the CH_2 sample was much longer than that for the carbon sample. Moreover, ^{241}Am sources were used to test the detectors and the DAQ system before, during, and after the experiment.

E. DAQ system

The experimental data were recorded using the Backn DAQ system [31], which contained binary data of waveforms from all the telescopes, including two kinds of signals: a) those from the Si detectors that were only pre-processed by preamplifiers, and b) those from the CsI detectors that were multiplied by SiPMs and then amplified by the main amplifiers.

III. PRINCIPLE OF MEASUREMENT

The ratios of the differential cross sections of the $^{12}\text{C}(n, xd)$ reactions to those of the n - p elastic scattering in the corresponding neutron energy bin E_n and at the outgoing angle θ_L were measured first, and the principle for the measurement is described in the following equation:

$$R(\theta_L, E_n) \equiv \frac{d\sigma/d\Omega(\theta_L, E_n) \Big|_{^{12}\text{C}(n, xd)}}{d\sigma/d\Omega(\theta_L, E_n) \Big|_{n-p \text{ scattering}}} = \frac{C_d(\theta_L, E_n) \cdot (1 - c_p^{\text{dead_time}}(\theta_L, E_n)) \cdot \varepsilon_p(\theta_L, E_n) \cdot N_H}{C_p(\theta_L, E_n) \cdot (1 - c_d^{\text{dead_time}}(\theta_L, E_n)) \cdot \varepsilon_d(\theta_L, E_n) \cdot N_{^{12}\text{C}}} \cdot f_{\text{beam}}, \quad (1)$$

where $R(\theta_L, E_n)$ is the ratio of the differential cross section of the $^{12}\text{C}(n, xd)$ reactions to those of the n - p scattering in the corresponding neutron energy bin E_n and at the outgoing angle θ_L . The determination of neutron energy intervals will be explained in detail in section 4.5. $C_d(\theta_L, E_n)$ is the net count of deuteron events from the $^{12}\text{C}(n, xd)$ reactions detected by the telescope at laboratory angle θ_L for neutron energy E_n . A correction of the influence from the ^{13}C on $C_d(\theta_L, E_n)$ was carried out. However, it was rather insignificant because the abundance of ^{12}C (98.93%) is 92.46 times that of ^{13}C (1.07%) [12], and the cross section of the $^{12}\text{C}(n, d)^{11}\text{B}$ reaction is at least 1.80 times bigger than that of the $^{13}\text{C}(n, d)^{12}\text{B}$ reaction according to the EAF-2010 library [32], which suggests that the deuterons from the $^{12}\text{C}(n, d)^{11}\text{B}$ reaction are at least 166 times more than those from the $^{13}\text{C}(n, d)^{12}\text{B}$. $C_p(\theta_L, E_n)$ is the net count of proton events from the n - p scattering. $c_d^{\text{dead_time}}(\theta_L, E_n)$ and $c_p^{\text{dead_time}}(\theta_L, E_n)$ are the respective correction factors due to the DAQ dead time for the carbon measurement and the n - p scattering measurement. They are determined by the portion of the saturated signals over the total number of the signals, which will be given in section IVA. $\varepsilon_d(\theta_L, E_n)$ is the detection efficiency for deuterons from the carbon sample, and $\varepsilon_p(\theta_L, E_n)$ is the detection efficiency for protons from the CH_2 sample, which will be discussed in section IVD. f_{beam} is the ratio of the number of protons bombarding the tungsten target (and thus producing neutrons) during the $^{12}\text{C}(n, xd)$ reactions measurement to that during the n - p scattering measurement. $N_{^{12}\text{C}}$ and N_H are the numbers of ^{12}C atoms in the graphite foil sample and hydrogen atoms in the CH_2 sample, respectively. For relative measurement, the neutron fluence term and the solid angle term are eliminated.

The study of n - p scattering was for the measurement of the relative differential cross sections of the n - p scattering, details of which can be found in Ref. [21]. The results were relative differential cross sections of the n - p scattering, but only the net counts of protons from the n - p scattering, $C_p(\theta_L, E_n)$, the dead time correction, $c_p^{\text{dead_time}}(\theta_L, E_n)$, and the detection efficiency for protons, $\varepsilon_p(\theta_L, E_n)$, were used in the present work to calculate $R(\theta_L, E_n)$ in Eq. (1).

As it is not convenient to compare the present results, $R(\theta_L, E_n)$, to the previous ones obtained directly, the differential cross sections of the $^{12}\text{C}(n, xd)$ reactions were thus calculated using the differential cross section data of

As it is not convenient to compare the present results, $R(\theta_L, E_n)$, to the previous ones obtained directly, the differential cross sections of the $^{12}\text{C}(n, xd)$ reactions were thus calculated using the differential cross section data of

the n - p scattering from the JENDL-4.0/HE-2015 library as the standard [22].

$$\left. \frac{d\sigma(\theta_L, E_n)}{d\Omega} \right|_{\text{lab}}^{^{12}\text{C}(n,xd)} = R(\theta_L, E_n) \cdot \left. \frac{d\sigma(\theta_L, E_n)}{d\Omega} \right|_{n-p \text{ scattering}}^{\text{JENDL-lab}}, \quad (2)$$

where $\left. \frac{d\sigma(\theta_L, E_n)}{d\Omega} \right|_{\text{lab}}^{^{12}\text{C}(n,xd)}$ are the differential cross sections of the $^{12}\text{C}(n, xd)$ reactions to be calculated in the laboratory system. $\left. \frac{d\sigma(\theta_L, E_n)}{d\Omega} \right|_{n-p \text{ scattering}}^{\text{JENDL-lab}}$ are the evaluated data of n - p scattering differential cross sections (in the laboratory system) extracted from the JENDL-4.0/HE-2015 [22] (= FENDL-3.1d [33]) library. The n - p

data extracted from the JENDL-4.0/HE-2015 library were originally given as Legendre polynomial coefficients in the center-of-mass (CM) system. Using the coefficients, the differential cross sections of the n - p scattering in the CM system can be calculated, and they are transformed to the data in the laboratory system, which are $\left. \frac{d\sigma(\theta_L, E_n)}{d\Omega} \right|_{n-p \text{ scattering}}^{\text{JENDL-lab}}$.

IV. DATA ANALYSIS

The method of the data analysis is similar to that for our n - p scattering measurement in 2019 [21]. A flow-chart demonstrating the process of data analysis is shown in Fig. 3.

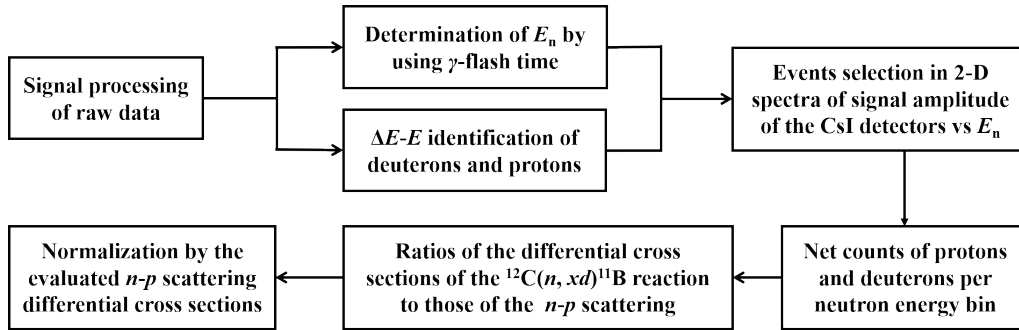


Fig. 3. Process of data analysis.

A. Signal processing

The recorded data of waveforms were processed and the amplitudes of the signals, the corresponding neutron TOF of each event, $c_d^{\text{dead_time}}(\theta_L, E_n)$, and $c_p^{\text{dead_time}}(\theta_L, E_n)$ in Eq. (1) were thus obtained. $c_d^{\text{dead_time}}(\theta_L, E_n)$ (<3%) are the portions of the saturated signals over the total number of the signals for the carbon sample measurement and $c_p^{\text{dead_time}}(\theta_L, E_n)$ (<2%) is that for the CH₂ sample measurement.

B. Determination of E_n using γ -flash time

The neutron energy for each event, E_n , is determined using the time-of-flight (TOF) method. γ -flash is produced in the spallation process and the γ -flash peak was used as the T_0 position. The TOF distributions of the γ -flash counts, i.e., the γ -flash event counts vs their TOFs for the Si-PIN detector and the CsI detector at $\theta_L = 15.1^\circ$, are presented in Fig. 4 (a) and (b), respectively, as examples. For each of the telescopes, the TOF distribution of the γ -flash events can be fitted by a double-peaked Gaussian distribution with a standard deviation of ~ 25 ns. This ~ 25 ns of standard deviation was caused by a) the width of the proton pulse that impinged on the tungsten target (main source), b) the time resolution of the detectors (several ns), and c) the time resolution of the DAQ

system (<1 ns). The absolute TOF of the neutron for each event can be calculated:

$$\text{TOF} = T_{\text{event}} - \left(T_0 - \frac{L}{c} \right), \quad (3)$$

where T_{event} is the starting time for the proton and deuteron events obtained from the Si-PIN signal because of its faster response time compared to the CsI signal. L is the length of the neutron flight path (57.99 m), and c is the velocity of light. The corresponding neutron energy for each event E_n can then be obtained from its TOF, where the relativistic effect is considered.

C. ΔE - E spectra for deuteron and proton identification

The ΔE - E distributions for all ten telescopes were obtained for the identification of the deuteron and proton events from the carbon sample and the CH₂ sample, respectively. The 2-D spectra of the ΔE - E signal amplitudes at $\theta_L = 15.1^\circ$ obtained from the carbon sample and from the CH₂ sample are shown in Fig. 5 (a) and (b), respectively as examples. The same 2-D spectra obtained from the empty target were also analyzed and they were all blank, which proved that there was no charged particle background from the radiation on the aluminum sample holder by the neutron beam or the neutron beam itself.

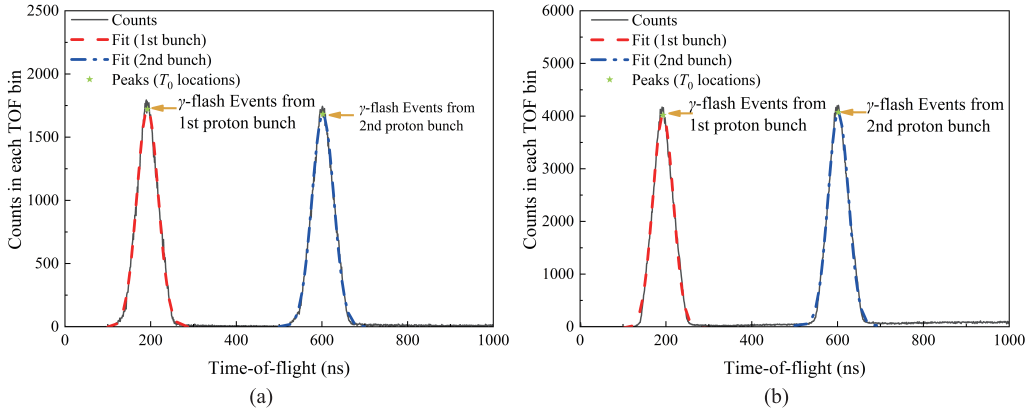


Fig. 4. (color online) TOF spectra of the γ -flash detected by the Si-PIN (a) and the CsI (b) detectors at $\theta_L = 15.1^\circ$. The semi-transparent red and blue lines are the fitting curves corresponding to the first and second proton bunches, respectively. The peak positions are shown as green stars.

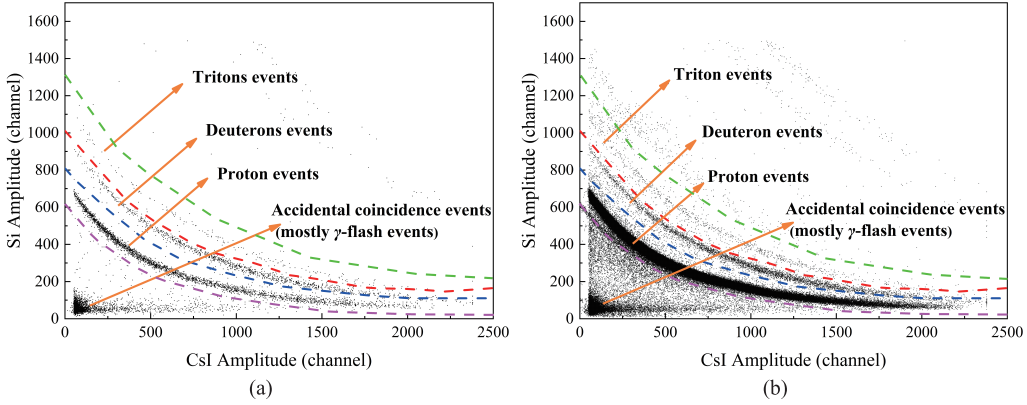


Fig. 5. (color online) 2-D distributions of the ΔE - E signal amplitudes at $\theta_L = 15.1^\circ$ from the carbon sample measurement (a) and the CH_2 sample measurement (b).

From Fig. 5 (a), it is clear that the number of proton events is much larger than the deuteron counts from the CH_2 sample. Therefore, the results from the CH_2 sample measurement are not suitable for obtaining the relative differential cross sections of the $^{12}\text{C}(n, xd)$ reactions because of the strong interference from the protons, although there are plenty of carbon atoms in the CH_2 sample. Taking the counts at $\theta_L = 15.1^\circ$ for instance, the number of proton events is 14.67 times that of deuteron events, which indicates that even a small number of protons misidentified by the boundaries (red lines and blue lines in Fig. 5 (b)) as deuterons will significantly affect the deuteron counts. This effect is particularly obvious for the area with high CsI detector signal amplitudes and low Si detector signal amplitudes, as can be seen in Fig. 5 (b). Consequently, a carbon sample (the graphite foil) was necessary for the present work for deuteron events measurement from the $^{12}\text{C}(n, xd)$ reactions. As shown in Fig. 5, the interference from the proton events was much less for the carbon sample than those for the CH_2 sample and the interference is apparent only for CsI detector signal amplitudes greater than 2000 channels, where the corresponding neutron energy is larger than 60 MeV and out of the

range of the present results.

D. 2-D spectra of signal amplitude of the CsI detectors vs E_n

With the knowledge of the neutron energy E_n for each deuteron or proton event and the signal amplitude of the CsI detectors, the 2-D distribution of the amplitude of the CsI detector output signal vs E_n (hereinafter referred to as the “CsI vs E_n spectrum”) is obtained. As the neutron source is double-bunched, the T_0 time for each of the two bunches is used to determine the corresponding neutron energy separately. The protons detected at $\theta_L = 15.1^\circ$ from the CH_2 sample are plotted in Fig. 6 (a) and (b) as the 2-D distribution of the signal amplitude of the CsI detectors signals vs E_n as an example, which correspond to the first and second bunch, respectively.

The identified deuterons using the ΔE - E method from the carbon sample are plotted as the 2-D distribution of the signal amplitude of the CsI detectors signals vs E_n . Fig. 7 (a) and (b) are the scatter plots of the detected deuteron distribution at $\theta_L = 15.1^\circ$ corresponding to the first and second bunches, respectively.

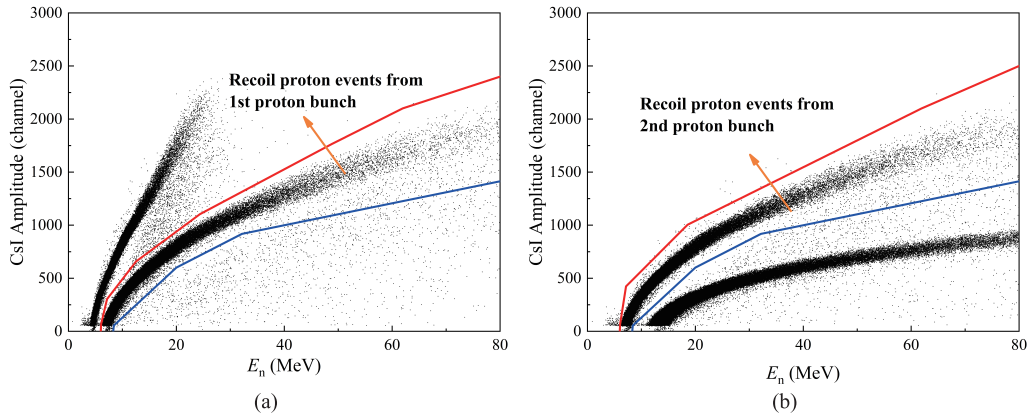


Fig. 6. (color online) 2-D distribution of the signal amplitude of the CsI detector vs neutron energy E_n at $\theta_L = 15.1^\circ$ for protons from the CH_2 sample. The neutron energy E_n corresponds to the first proton bunch in (a) and the second proton bunch in (b). The red line and the blue line are the upper and lower boundaries of the valid event area, respectively.

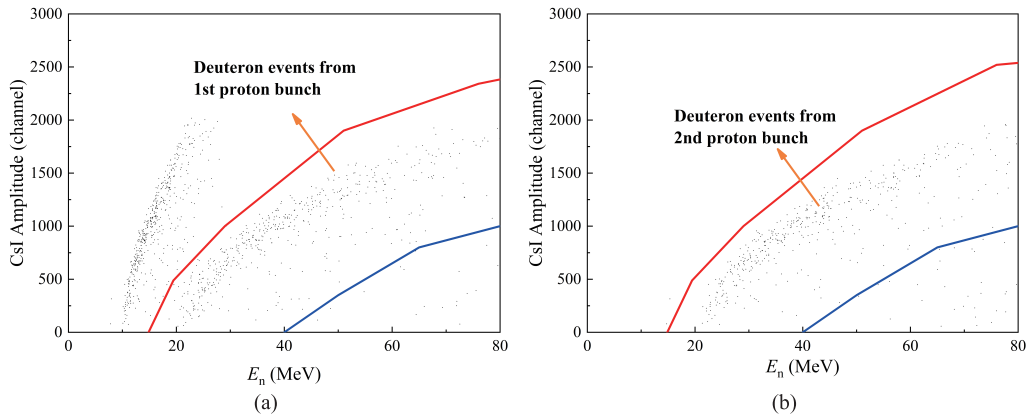


Fig. 7. (color online) 2-D distribution of the signal amplitude of the CsI detector vs neutron energy E_n at $\theta_L = 15.1^\circ$ for deuterons using the ΔE - E method from the carbon sample. The neutron energy, E_n , corresponds to the first proton bunch in (a) and the second proton bunch in (b). The red line and the blue line are the upper and lower boundaries of the valid event area.

As is shown in Fig. 7, the area of the deuteron events is not clear for both the first and second bunches, which creates considerable difficulty in selecting the boundaries of the deuteron events and in determining the detection efficiency for the deuterons. Consequently, the selection of the boundaries is a vital source of uncertainty of the result. The experimental results of the $^{12}\text{C}(n, d)^{11}\text{B}$ reactions given in the present work include deuterons corresponding to different energy levels from multiple reactions such as ^{11}B (ground state, excited states of 2.12, 4.44, 5.02, 6.74, and 6.79 MeV) from the $^{12}\text{C}(n, d)^{11}\text{B}$ reaction. As a result, the boundaries of the deuterons were drawn noticeably wider than those of the protons (as shown in Fig. 6 and Fig. 7) to guarantee a high detection efficiency for deuterons, $\varepsilon_d(\theta_L, E_n)$, which was viewed as 100%. Although this approximation may introduce random events, it was reasonable and necessary. Furthermore, the boundaries were drawn narrower in the error analysis. The different counts between the narrow boundaries and the wide boundaries were counted as a source of uncertainty. The errors introduced by the random events

and those by the approximation of viewing $\varepsilon_d(\theta_L, E_n)$ as 100% were thus included in the uncertainty of the boundaries. For the protons from the n - p scattering, it was found that $\varepsilon_p(\theta_L, E_n) > 98\%$ by using the Monte Carlo simulation and comparing the experimental spectrum with that from the simulation. The method of the simulation is described in detail in Ref. [30]. The result $\varepsilon_p(\theta_L, E_n) > 98\%$ was first reported in Ref. [21].

E. Counts per E_n bin

The neutron energy E_n for the Back-n white neutron source is split into six bins in the present work with a TOF interval of 50 ns according to the ~ 25 ns standard deviation of the Gaussian distribution of the γ -flash events, as described in section IVB. The E_n values in the present work, 25.2 MeV, 28.6 MeV, 32.7 MeV, 37.8 MeV, 44.2 MeV, and 52.5 MeV, are midpoints of their corresponding intervals. The differences between each midpoint and the boundaries of their intervals are thus viewed as the uncertainties of E_n . The Q -value of the $^{12}\text{C}(n, d)^{11}\text{B}$ reaction is -13.732 MeV and the reaction

threshold is 14.887 MeV [34]. The energies of the corresponding deuterons from the $^{12}\text{C}(n, d)^{11}\text{B}$ reaction are 9.7 to 38.4 MeV for the ground state of ^{11}B according to binary reaction dynamics. Other channels, such as the $^{12}\text{C}(n, n+d)$, etc., have Q -values lower than -13.732 MeV and therefore higher thresholds than 14.887 MeV. These higher thresholds, combined with the kinematics of the deuteron production reactions other than the $^{12}\text{C}(n, d)^{11}\text{B}$ reaction, suggest that the emitting deuterons have lower energies than the deuterons from the $^{12}\text{C}(n, d)^{11}\text{B}$ reaction for the ground state ^{11}B . The lower limit of the neutron energy for the present work is 25.2 MeV because of the negative Q -value of the $^{12}\text{C}(n, d)^{11}\text{B}$ reaction [34] and the energy loss in the ΔE layer (Si-PIN detector) for particle identification. The upper limit of neutron energy is 52.5 MeV because the uncertainty of E_n increases and the number of recoil protons from the n - p scattering is not adequate due to the small cross sections of the n - p scattering and the weak neutron beam flux for $E_n > 52.5$ MeV [21]. The signal amplitudes caused by higher-energy protons are beyond the input voltage range of the DAQ system for the CsI detectors of the telescopes at $\theta_L = 10.1^\circ$ and $\theta_L = 15.1^\circ$. As a result, there are no data for the $^{12}\text{C}(n, xd)$ reactions $\theta_L = 10.1^\circ$, and the upper limit is 44.2 MeV at $\theta_L = 15.1^\circ$ [21]. The numbers of protons from the CH_2 sample and those of the deuterons from the carbon sample within the boundaries drawn in section IVD, $C_p(\theta_L, E_n)$ and $C_d(\theta_L, E_n)$ in Eq. (1), are counted into the corresponding neutron energy bin according to the neutron energy. The numbers of protons from the CH_2 sample and those of the deuterons from the carbon sample within the boundaries drawn in section IVD, $C_p(\theta_L, E_n)$ and $C_d(\theta_L, E_n)$ in Eq. (1), are counted into the corresponding neutron energy bins according to the neutron energy.

$C_d(\theta_L, E_n)$ is the net count of the deuterons, which is the count for graphite foil measurement subtracted by the count for empty target measurement (normalized according to the beam of protons of the accelerator). However, there were no deuteron events in the empty target measurement run; therefore, the counts from the carbon sample measurement were the net counts. The net count of the protons from the CH_2 sample, $C_p(\theta_L, E_n)$, can be obtained after the background subtraction, which is described in detail in Ref. [21]. Because of the small cross sections and negative Q -values (-12.59 MeV for the $^{12}\text{C}(n, p)^{12}\text{B}$ reaction, for instance) [34] of the $^{12}\text{C}(n, xp)$ reactions, the proton background from the $^{12}\text{C}(n, xp)$ reactions is very weak compared to the protons from the n - p scattering. The spectrum of signal amplitude vs. net counts of protons from the CH_2 sample and that of deuterons from the carbon sample within the boundaries of the $E_n = 44.2$ MeV energy bin detected by the CsI detector at $\theta_L = 15.1^\circ$ is presented in Fig. 8 as an example.

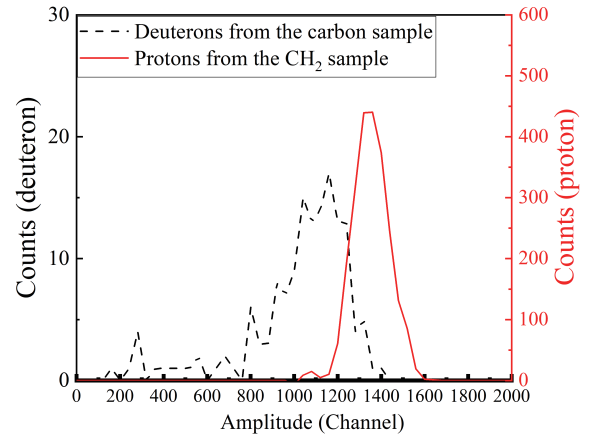


Fig. 8. (color online) Counts vs amplitude of the CsI detector signal at $\theta_L = 15.1^\circ$ for the net deuterons from the carbon sample and the net protons from the CH_2 sample in the $E_n = 44.2$ MeV bin. Note that the scales for the deuteron counts (left black Y-axis) and the proton counts (right red Y-axis) are different. Counts in every 40 channels are added up.

F. Ratios of the differential cross sections of the $^{12}\text{C}(n, xd)$ reactions to those of the n - p scattering

The ratios of the differential cross sections of the $^{12}\text{C}(n, xd)$ reactions to those of the n - p scattering, $R(\theta_L, E_n)$, can be calculated according to Eq. (1). As the present work is a relative measurement, $N_H/N_{^{12}\text{C}}$ can be calculated using the following equations:

$$\frac{N_H}{N_{^{12}\text{C}}} = \frac{\rho_{\text{CH}_2} \cdot d_{\text{CH}_2} / M_{\text{CH}_2}}{2 \cdot \rho_{\text{graphite}} \cdot d_{\text{graphite}} \cdot a_{^{12}\text{C}} / M_{\text{NatC}}}, \quad (4)$$

where $\rho_{\text{graphite}} = 1.80 \text{ g/cm}^3$ and $\rho_{\text{CH}_2} = 0.92 \text{ g/cm}^3$ are the densities of the carbon sample and the CH_2 sample, respectively, as provided by the manufacturer. $d_{\text{graphite}} = 0.049 \text{ mm}$ is the thickness of the carbon sample and $d_{\text{CH}_2} = 0.103 \text{ mm}$ is the thickness of the CH_2 sample, both of which were measured using a micrometer. The areas of both samples were eliminated because the incident neutron beam spot was well covered by the samples. $M_{\text{NatC}} = 12.0 \text{ g/mol}$ is the molecular mass of natural carbon element, and $M_{\text{CH}_2} = 14.0 \text{ g/mol}$ is the molecular mass of CH_2 . $a_{^{12}\text{C}} = 98.93\%$ is the abundance of ^{12}C [12].

G. Normalization by the evaluated n - p scattering differential cross sections

To compare the results from the present work with the previous ones from the literature [9, 13, 16–18] and the data from theoretical calculations [19], differential cross sections of the $^{12}\text{C}(n, xd)$ reactions are obtained using the measured data $R(\theta_L, E_n)$ and the evaluated n - p scattering differential cross sections from the JENDL-4.0/HE-2015 library for normalization [22], as described in Eq. (2).

V. RESULTS AND DISCUSSION

The measured differential cross sections in the laboratory system are presented in Fig. 9 and the tabulated data are given in Table 2. Brenner's theoretical calculations using INCA code [16, 19] are also included in Fig. 9. The INCA code calculates the pre-equilibrium process using the intranuclear cascade model and describes the deexcitation of the compound nucleus based on the Fermi-break-up model [19, 35]. In addition, the data using Talys-1.9 code with default parameters [36] were calculated in the present work, and the results are presented in each plot. The data from the JENDL-4.0/HE-2015 library [22, 37] and the ENDF-B/VIII.0 library [38] are also included in Fig. 9, all of which were calculated based on GNASH code [39]. Furthermore, the results from previous measurements are also presented for comparison. There are only nine previous measurements [1, 2, 9, 13, 16-18, 40, 41] recorded in the EXFOR library, seven of which are in the several tens of MeV range [1, 2, 9, 13, 16-18] and five of which are within the neutron energy region of the present work. Those five measurement results are included in Fig. 9 for comparison. Some of the previous measurements were for the double differential cross sections of the deuteron production reactions on carbon, and they were energy-integrated to obtain angle-differential cross sections for comparison. Young's original results were given for three energy levels of ^{11}B in the $^{12}\text{C}(n, d)^{11}\text{B}$ reaction (ground state, level 1, and level 2 of ^{11}B) [18], and the differential cross sections of the three levels are added up in Fig. 9 (f) as "combined."

The sources of uncertainties and their magnitudes for the present work are listed in Table 3. Note that the uncertainties of the counts of the n - p scattering are included in the present work because the proton counts were used for the relative measurement [33].

The relatively short beam duration did not help obtain sufficiently good statistics and made it difficult to determine the valid area of the deuteron events in the 2-D spectrum scatter plots, including the ΔE - E spectra and the E_n -CsI spectra, as presented in Fig. 7 and Fig. 5 (a). This consequently brought about a rather large overall uncertainty. In addition, the uncertainty of E_n , i.e., the horizontal error shown in Table 3, is half the value of the width of the E_n interval, as explained in section IVE. The horizontal error increases as E_n increases.

As shown in Fig. 9, for all six energy regions, 25.3 ± 1.5 , 28.6 ± 1.9 , 32.7 ± 2.3 , 37.8 ± 2.8 , 44.2 ± 3.6 , and 52.5 ± 4.7 MeV, the differential cross sections measured in the present work monotonically decline as θ_L increases. For $E_n = 28.6 \pm 1.9$ MeV, the present results favor the data of Slypen et al. at $E_n = 29.5$ MeV [13], while the data by Subramanian et al. at $E_n = 27.4$ MeV [16] are noticeably larger with fluctuations in magnitude. From

32.7 MeV to 37.8 MeV, the present results agree well with the data of Slypen *et al.* [13] and Subramanian *et al.* [16]. The present results show a strong forward-peaked nature and fall drastically with the increase of θ_L , which is supported by all the results from the previous measurements. This effect is better characterized by the INCA code theoretical calculations by Brenner *et al.* [19], although the calculations predict results higher than the present ones and the previous measurement data at forward angles [13]. In addition, the decrease in the results as θ_L increases from the Talys-1.9 code, the JENDL-4.0/HE-2015 library, and the ENDF-B/VIII.0 is much milder.

The present data generally agree with the previous measurements except for the data of McNaughton at $E_n = 56.0$ MeV [9]. As shown in Fig. 9 (f), McNaughton's data are larger than most of the other results, especially for $\theta_L \leq 40^\circ$, while the present results are in better agreement with the data of Slypen *et al.* [13]. In contrast, Young's data for the $^{12}\text{C}(n, d)^{11}\text{B}$ reaction at 60.0 MeV [18] are significantly smaller than the rest, including the experimental data and all the theoretical calculations, which gives a scope of the contribution of the $^{12}\text{C}(n, d)^{11}\text{B}$ reaction to the deuteron production from carbon. The data from the INCA code theoretical calculations at 40 MeV are larger than the present data and the previous measurements at the forward angles; however, they are in good accordance with the present results and the previous ones for $\theta_L \geq 25^\circ$.

In general, despite the relatively large uncertainties, the present results agree with most of the previous experimental data relatively well considering the error bars in the whole energy region. The present results also agree with those of the theoretical calculations by Brenner *et al.* [19] at large emission angles and in higher neutron energy regions ($\theta_L > 30^\circ$ and $E_n > 40$ MeV).

VI. CONCLUSIONS

In the present paper, the angle-differential cross sections of the $^{12}\text{C}(n, xd)$ reactions relative to those of the n - p scattering at six neutron energies from 25 MeV to 52 MeV are measured at the CSNS back-n white neutron source. Moreover, the present work includes theoretical calculations using the Talys-1.9 code with default parameters. Both the measured and the calculated results are compared with the data from the previous measurements, the evaluated data from the JENDL-4.0/HE-2015 library and the ENDF-B/VIII.0 library using GNASH code, and those from theoretical calculations based on INCA code. The measured results agree with most of the previous measurements in terms of the trend and magnitude (except for Young's dedicated data for the $^{12}\text{C}(n, d)^{11}\text{B}$ reaction) in the neutron energy region of the present work and

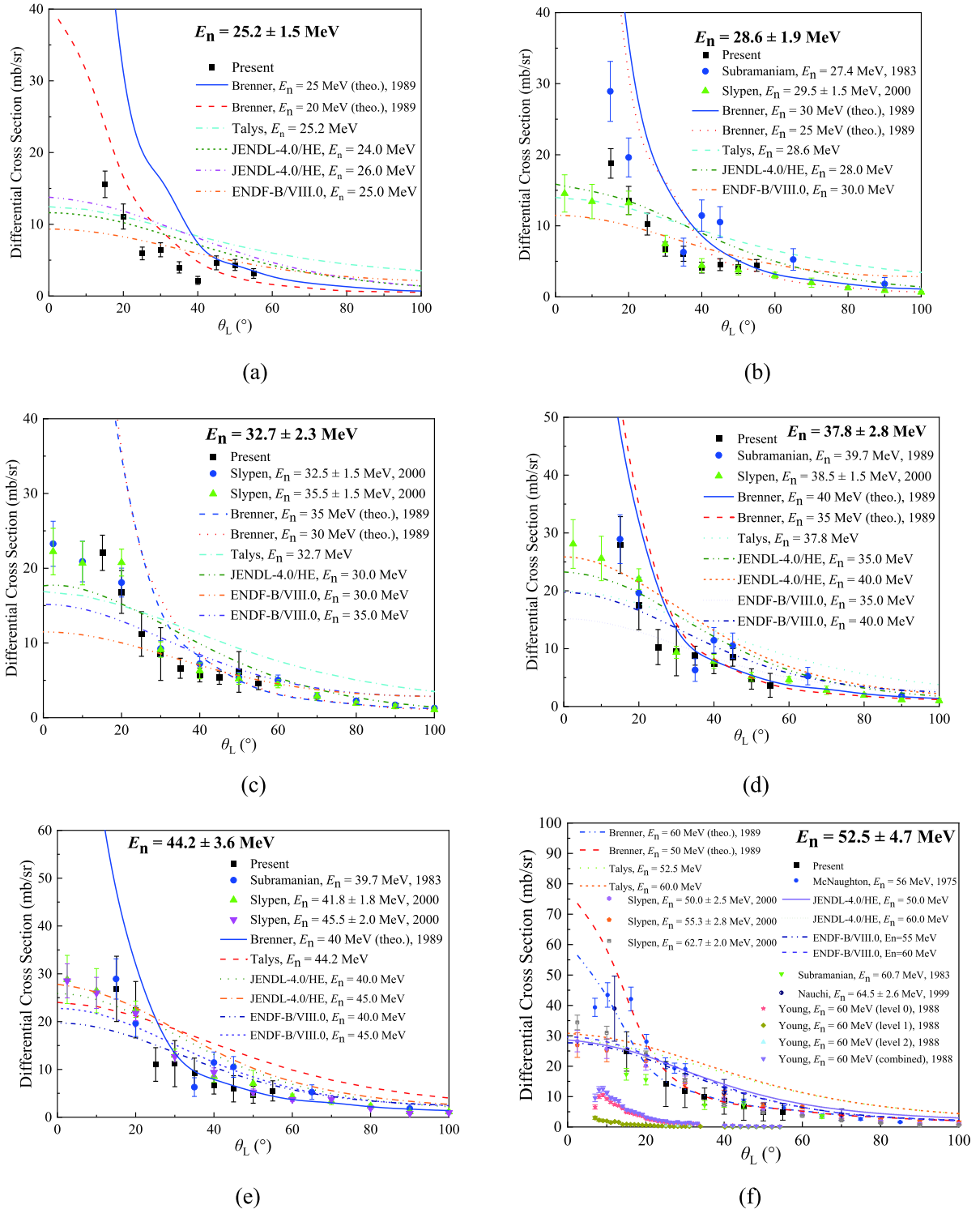


Fig. 9. (color online) Differential cross sections of the $^{12}\text{C}(n, xd)$ reactions measured at $E_n = 25.2$ MeV, 28.6 MeV, 32.7 MeV, 37.8 MeV, 44.2 MeV, and 52.5 MeV compared with results from previous measurements, the evaluated data, and the theoretical calculations. The previous experimental results were taken from the EXFOR library [14] and they include those of Subramanian *et al.* 1983 [16], Slypen *et al.* 2000, McNaughton *et al.* 1975 [9], Nauchi *et al.* 1999 [17], and Young *et al.* 1988 [18]. The evaluated data were taken from the JENDL-4.0/HE-2015 library [22, 37] and the ENDF-B/VIII.0 library [38], which were all calculated using GNASH code [39]. The theoretical calculations were carried out by Brenner *et al.* [19]. The calculations in the present work were based on the Talys-1.9 code [36]. The purple triangles in (f) are the combined data of Young (1988) at $E_n = 60.0$ MeV [18] for level 0, level 1, and level 2 of ^{11}B .

Table 2. Measured results of the $^{12}\text{C}(n, xd)$ reactions. $R(\theta_L, E_n)$ are the ratios of the differential cross sections of the $^{12}\text{C}(n, xd)$ reactions to those of the n - p scattering. $\frac{d\sigma(\theta_L, E_n)}{d\Omega}|_{^{12}\text{C}(n, xd)}^{\text{lab}}$ are the differential cross sections of the $^{12}\text{C}(n, xd)$ reactions normalized by the JENDL-4.0/HE-2015 [22] data of the n - p scattering.

θ_L ($^\circ$)	$E_n = 25.2 \pm 1.5$ MeV		$E_n = 28.6 \pm 1.9$ MeV		$E_n = 32.7 \pm 2.3$ MeV	
	$R(\theta_L, E_n)$	$\frac{d\sigma(\theta_L, E_n)}{d\Omega} _{^{12}\text{C}(n, xd)}^{\text{lab}}$	$R(\theta_L, E_n)$	$\frac{d\sigma(\theta_L, E_n)}{d\Omega} _{^{12}\text{C}(n, xd)}^{\text{lab}}$	$R(\theta_L, E_n)$	$\frac{d\sigma(\theta_L, E_n)}{d\Omega} _{^{12}\text{C}(n, xd)}^{\text{lab}}$
15.1	0.122±0.015	15.6±1.8	0.168±0.019	18.8±2.1	0.228±0.024	22.1±2.4
20.0	0.092±0.015	11.1±1.7	0.129±0.019	13.6±2.0	0.186±0.032	16.8±2.9
25.1	0.052±0.008	5.94±0.89	0.104±0.016	10.2±1.5	0.133±0.035	11.2±3.0
30.0	0.061±0.009	6.45±0.98	0.073±0.011	6.7±1.0	0.110±0.045	8.5±3.5
35.0	0.041±0.008	3.99±0.79	0.072±0.013	6.1±1.1	0.092±0.019	6.6±1.3
40.0	0.024±0.006	2.18±0.55	0.053±0.010	4.12±0.76	0.089±0.014	5.72±0.93
45.0	0.057±0.012	4.62±0.97	0.065±0.012	4.54±0.82	0.091±0.015	5.35±0.88
50.0	0.059±0.010	4.33±0.77	0.066±0.014	4.18±0.88	0.115±0.051	6.1±2.7
55.0	0.047±0.010	3.14±0.67	0.077±0.014	4.43±0.83	0.095±0.018	4.63±0.88

θ_L ($^\circ$)	$E_n = 37.8 \pm 2.8$ MeV		$E_n = 44.2 \pm 3.6$ MeV		$E_n = 52.5 \pm 4.7$ MeV	
	$R(\theta_L, E_n)$	$\frac{d\sigma(\theta_L, E_n)}{d\Omega} _{^{12}\text{C}(n, xd)}^{\text{lab}}$	$R(\theta_L, E_n)$	$\frac{d\sigma(\theta_L, E_n)}{d\Omega} _{^{12}\text{C}(n, xd)}^{\text{lab}}$	$R(\theta_L, E_n)$	$\frac{d\sigma(\theta_L, E_n)}{d\Omega} _{^{12}\text{C}(n, xd)}^{\text{lab}}$
15.1	0.339±0.060	27.9±4.9	0.390±0.099	26.8±6.8	0.43±0.11	24.8±6.5
20.0	0.228±0.055	17.5±4.2	0.356±0.093	22.5±5.9	–	–
25.1	0.146±0.043	10.3±3.0	0.190±0.061	11.0±3.5	0.30±0.15	14.1±7.4
30.0	0.149±0.066	9.6±4.3	0.213±0.092	11.2±4.8	0.28±0.13	12.0±5.6
35.0	0.150±0.028	8.8±1.6	0.195±0.067	9.2±3.2	0.268±0.075	10.0±2.8
40.0	0.141±0.033	7.4±1.8	0.159±0.044	6.7±1.8	0.27±0.14	8.7±4.5
45.0	0.179±0.033	8.5±1.5	0.158±0.073	5.9±2.7	0.23±0.15	6.7±4.5
50.0	0.110±0.041	4.8±1.8	0.136±0.051	4.7±1.8	0.18±0.11	4.9±2.8
55.0	0.090±0.051	3.7±2.1	0.170±0.065	5.5±2.1	0.19±0.11	5.0±2.7

Table 3. Sources of uncertainties and their magnitudes.

Sources of the uncertainty	Magnitude (%)
Statistical error of deuteron counts ($C_d(\theta_L, E_n)$)	8.3 – 25.0
AE - E identification of deuterons ($C_d(\theta_L, E_n)$)	1.1 – 39.7
Deuteron event selection in the 2-D spectra of the CsI vs E_n plots ($C_d(\theta_L, E_n)$)	1.4 – 53.4
Uncertainty from the measurement of proton counts from the CH_2 sample ($C_p(\theta_L, E_n)$) [21]	2.7 – 5.3
Uncertainty from N_H	2.0
Uncertainty from N_C	2.0
E_n (horizontal error)	6.0 – 9.0
Overall uncertainty	10.3 – 66.8

are in accordance with the theoretical calculations by Brenner *et al.* at $E_n = 50$ and 60 MeV. The present work is the first white-neutron-source-based measurement of angular-differential cross sections of $^{12}\text{C}(n, xd)$ reactions in the several tens of MeV range. The present results provide relative differential cross section data at a wider neutron energy range from 25 MeV to 52 MeV than the previous ones, all of which are obtained using mono-energetic neutrons.

ACKNOWLEDGEMENTS

The authors are grateful to the operating crew of the CSNS white neutron source. Senior Engineer Yongli Jin from the China Institute of Atomic Energy is appreciated for the support in data reading from the ENDF-B/VIII.0 library. The authors would also like to thank Prof. Zhenpeng Chen from Tsinghua University for valuable discussions.

References

- [1] U. Tippawan, S. Pomp, J. Blomgren *et al.*, *Phys. Rev. C* **79**(6), 064611 (2009)
- [2] B. E. Bergenwall, A. Ataç, and S. Kullander, *Nucl. Phys. A* **747**(2), 152-181 (2005)
- [3] J. P. Meulders, S. Benck, I. Slypen *et al.*, *Med. Phys.* **27**(11), 2541-2559 (2000)
- [4] S. Dangtip, A. Ataç, B. Bergenwall *et al.*, *Nucl. Instrum. Methods Phys. Res. A* **452**(3), 484-504 (2000)
- [5] J. Blomgren and N. Olsson, *Radiat. Prot. Dosim.* **103**(4), 293-304 (2003)
- [6] D. L. Schwartz, J. Einck, J. Bellon *et al.*, *Int. J. Radiation Oncology Biol. Phys.* **50**(2), 449-456 (2001)
- [7] G. B. Moffitt, R. D. Stewart, G. A. Sandison *et al.*, *Physics in Medicine and Biology* **63**(10), (2018)
- [8] J. K. Rockhill and G. E. Laramore. *Neutron Radiotherapy*. Elsevier, Philadelphia, 2016.
- [9] M. W. McNaughton, N. S. P. King, F. P. Brady *et al.*, *Nucl. Instrum. Methods* **129**(1), 241-245 (1975)
- [10] M. Pillon, M. Angelone, A. Krása *et al.*, *AIP Conf. Proc.* **1412**(1), 121-128 (2011)
- [11] M. Majerle, M. Angelone, A. Krása *et al.*, *Nucl. Instrum. Methods Phys. Res. A* **951**, 163014 (2020)
- [12] NuDat 2.8: nuclear structure and decay data., <https://www.nndc.bnl.gov/nudat2/>.
- [13] I. Slypen, S. Benck, J. P. Meulders *et al.*, *At. Data Nucl. Data Tables* **76**(1), 26-48 (2000)
- [14] EXFOR: Experimental Nuclear Reaction Data, <https://www-nds.iaea.org/exfor/exfor.htm>.
- [15] I. Slypen, V. Corcalciuc, and J. P. Meulders, *Phys. Rev. C* **51**(3), 1303-1311 (1995)
- [16] T. S. Subramanian, J. L. Romero, F. P. Brady *et al.*, *Phys. Rev. C* **28**(2), 521-528 (1983)
- [17] Y. Nauchi, M. Baba, T. Sanami *et al.*, *J Nucl. Sci. Technology* **36**(2), 143-151 (1999)
- [18] J.C.Young, F.P.Brady, J.L.Romero *et al.*, *Bull. Am. Phys. Soc.* **33**, (1988)
- [19] D. J. Brenner and R. E. Prael, *At. Data Nucl. Data Tables* **41**(1), 71-130 (1989)
- [20] H. T. Jing, J. Y. Tang, H. Q. Tang *et al.*, *Nucl. Instrum. Methods Phys. Res. A* **621**(1), 91-96 (2010)
- [21] H. Jiang, W. Jiang, Z. Cui *et al.*, *Eur. Phys. J. A* **57**(1), 6 (2021)
- [22] K. Shibata, O. Iwamoto, T. Nakagawa *et al.*, *J Nucl. Sci. Technology* **48**(1), 1-30 (2011)
- [23] H. Bai, R. Fan, H. Jiang *et al.*, *Chin. Phys. C* **44**(1), 014003 (2020)
- [24] Y. Chen, G. Luan, J. Bao *et al.*, *Eur. Phys. J. A* **55**(7), 115 (2019)
- [25] Q. An, H. Y. Bai, J. Bao *et al.*, *JINST* **12**(7), P07022-P07022 (2017)
- [26] MSI-8, <https://www.mesytec.com/products/datasheets/MSI-8.pdf>.
- [27] P. Eraerds, M. Legré, A. Rochas *et al.*, *Opt. Express* **15**(22), 14539-14549 (2007)
- [28] R. Fan, H. Jiang, W. Jiang *et al.*, *Nucl. Instrum. Methods Phys. Res. A* **981**, 164343 (2020)
- [29] W. Jiang, H. Bai, H. Jiang *et al.*, *Nucl. Instrum. Methods Phys. Res. A* **973**, 164126 (2020)
- [30] Z. Cui, H. Bai, H. Jiang *et al.*, EPJ Web Conf., *Proceedings of the International Conference on Nuclear Data for Science and Technology*, <https://doi.org/10.1051/epjconf/202023901039>.
- [31] B. He, P. Cao, D. L. Zhang *et al.*, *Chin. Phys. C* **41**(1), 016104 (2017)
- [32] EAF-2010: European Activation File, <https://www-nds.iaea.org/exfor/endlf.htm>.
- [33] FENDL-3.1d: Fusion Evaluated Nuclear Data Library Ver.3.1d, <https://www-nds.iaea.org/fendl/>.
- [34] Q-valueCalculator(QCalc),<https://www.nndc.bnl.gov/qcalc/>.
- [35] G. J. Mathews, B. G. Glagola, R. A. Moyle *et al.*, *Phys. Rev. C* **25**(5), 2181-2195 (1982)
- [36] A. J. Koning and D. Rochman, *Nuclear Data Sheets* **113**(12), 2841-2934 (2012)
- [37] S. Kunieda, O. Iwamoto, and N. Iwamoto. JAEA-Conf 2016-004, pp. 41-46 (2016)
- [38] D. A. Brown, M. B. Chadwick, R. Capote *et al.*, *Nuclear Data Sheets* **148**, 1-142 (2018)
- [39] P. G. Young and E. D. Arthur, *Los Alamos Scientific Lab. Reports*, No.7269-MS (1977).
- [40] P. J. Riley, C. W. Bjork, C. R. Newsom *et al.*, *Phys. Rev. C* **17**(5), 1881-1884 (1978)
- [41] J. Franz, E. Rössle, C. Sauerwein *et al.*, *Nucl. Phys. A* **472**(4), 733-758 (1987)